frontiers | Frontiers in Chemical Engineering

TYPE Original Research
PUBLISHED 23 September 2024
DOI 10.3389/fceng.2024.1439400



OPEN ACCESS

EDITED BY
Leilei Dai,
University of Minnesota Twin Cities,
United States

REVIEWED BY
Rui Ma,
Zhejiang Normal University, China
Marco A. Sanchez-Castillo,
Universidad Autónoma de San Luis Potosí,
Mexico

*CORRESPONDENCE
Kevin M. Van Geem,
Kevin.VanGeem@UGent.be

RECEIVED 27 May 2024
ACCEPTED 05 September 2024
PUBLISHED 23 September 2024

CITATION
He Q, Akin O, Ureel Y, Yazdani P, Li L, Varghese RJ and Van Geem KM (2024) Enhancing catalytic pyrolysis of polypropylene using mesopore-modified HZSM-5 catalysts: insights and strategies for improved performance.
*Front. Chem. Eng.* 6:1439400.
doi: 10.3389/fceng.2024.1439400



# Enhancing catalytic pyrolysis of polypropylene using mesopore-modified HZSM-5 catalysts: insights and strategies for improved performance

Qing He, Oguzhan Akin, Yannick Ureel, Parviz Yazdani, Lingfeng Li, Robin John Varghese and Kevin M. Van Geem*

Laboratory for Chemical Technology (LCT), Department of Materials, Textiles and Chemical Engineering, Faculty of Engineering and Architecture, Ghent University, Ghent, Belgium

Designing an active, selective, and stable catalyst for catalytic polyolefin pyrolysis is crucial for enhancing energy efficiency and economic viability in chemical processes. In this study, two synthesis methods—NaOH and NaOH/CTAB treatments—were employed to modify the physicochemical properties of CBV23, CBV55, and CBV80 zeolites. The catalytic performance of both parent and modified zeolites was evaluated for polypropylene pyrolysis using a two-stage micro-pyrolyzer coupled with two-dimensional GC-FID/MS. The NaOH/CTAB treatment preserved and enhanced strong acid sites while promoting a more uniform mesopore distribution. Among the catalysts tested, the hierarchical CBV80-ZM exhibited the best performance, achieving a propylene yield of 41 wt% and total light olefin and MA yields of 92 wt%. The improved catalytic performance was attributed to optimized acidity and larger pore size, which reduced the number of weak acid sites. These findings offer valuable insights for designing tailored zeolites based on specific target products for catalytic pyrolysis of plastic waste, particularly in the production of propylene and other high-value chemicals.

KEYWORDS

**catalytic pyrolysis, plastic wastes, zeolite, hierarchical catalyst, light olefins**

## 1 Introduction

Plastic products are ubiquitous in everyday life. Currently, global production of plastic exceeds 400 million tons annually (Wang et al., 2024). The widespread use of plastic has led to serious environmental pollution. In the context of global climate change and carbon reduction efforts, plastic recycling has attracted considerable attention across both academic and industrial sectors (Aristizábal-Lanza et al., 2022; Hussain et al., 2022). Catalytic pyrolysis stands as a promising method for plastic recycling, especially polyolefin waste, capable of transforming polymers into high-value chemicals such as $C_2$-$C_4$ light olefins (LO) and monoaromatics (MA) (Eschenbacher et al., 2022). Compared with traditional thermal pyrolysis, catalytic pyrolysis is more energy efficient and yields higher selectivities towards

LO and MA, thereby reducing the product's carbon footprint (Eschenbacher et al., 2022).

Catalytic pyrolysis technology relies on high-performance catalysts. Zeolites, specifically, are efficient catalysts for plastic catalytic pyrolysis (Dai et al., 2022). *In-situ* and *ex-situ* catalysis are two typical processes. In *in-situ* catalysis, the catalyst is in contact with the polymer melt. Conversely, in *ex-situ* catalytic pyrolysis, the thermal pyrolysis volatiles from the first reactor undergo further conversion in a second reactor with a catalyst bed (Abbas-Abadi et al., 2023). The *ex-situ* catalytic pyrolysis prevents direct contact between feed and catalyst and eliminates pore blockage caused by polymer melting and hence is preferred over *in-situ* catalytic pyrolysis. The commercial HZSM-5 catalyst is a typical microporous catalyst, with its unique pore structure primarily facilitating the entry of linear and isoparaffins and MA into its internal volume (Derouane, 1980). However, the active Brønsted acid sites (BAS) and Lewis acid sites within the HZSM-5 micropores are inaccessible to the large-branched molecules from plastic thermal pyrolysis (Dapsens et al., 2015). These molecules, like alkanes, alkenes, and naphthenes, cannot easily diffuse into the HZSM-5 micropores and are mostly subjected to cracking at the pore mouth. This will eliminate the pore-confinement effect for selective conversion, reduce the catalyst activity, and may lead to coke formation and catalyst deactivation. Therefore, the introduction of mesopores is necessary to effectively tailor catalyst performance towards a high yield to valuable base chemicals (Eschenbacher et al., 2022; Matsuura et al., 2022).

Hierarchical zeolites are a specific class of mesoporous zeolites, which consist of an ordered structure of micropores, mesopores, and even macropores (Na et al., 2013). In contrast to the pure mesopore catalyst, like MCM-41, these hierarchical catalysts offer advantages, including facilitating the diffusion of large molecules and enhancing selectivity through uniform space restriction (Akin et al., 2023). Hierarchical catalysts can improve MA production through pore-confinement, even without metal impregnation. Various synthesis methods for this catalyst have been developed, such as post-treatment through alkali leaching and pre-treatment using templating agent introduction (Eschenbacher et al., 2021). An example of a hierarchical pore structure catalyst is the core-shell catalyst HZSM-5/MCM-41, which involves assembling HZSM-5 seeds using cetyltrimethyl ammonium bromide (CTAB). Carcia et al. employed a batch reactor to study this zeolite for *in-situ* HDPE pyrolysis (García et al., 2005). The HZSM-5/MCM-41 maintained similar activity to pure HZSM-5 at 380°C and improved the light olefins selectivity. Enhanced production of gasoline-range hydrocarbons and aromatics was achieved by controlling the crystallization time during the synthesis of lignin-derived hierarchical HZSM-5 (Qian et al., 2021). This synthesis method compared to the CTAB-based method was more selective to aromatics due to its efficiency in preserving the catalyst acidity during lignin-based reassembly. Guo et al. (2022) prepared the HZSM-5/MCM-41 catalyst for upgrading cellulose vapors. The selectivity towards MA was increased by controlling the NaOH concentration to adjust the pore size and catalyst acidity. Groen et al. recommend using MFI zeolites with a Si/Al ratio of 25–50 for introducing mesopores with pure alkaline solutions (Groen et al., 2004a). Currently, the HZSM-5/MCM-41 catalyst has demonstrated excellent performance in alkylation of aromatics (Shen et al., 2021; Wang et al., 2022), biomass pyrolysis (Yu et al., 2020; Li et al., 2021), methanol conversion (Tang et al., 2012), etc. However, to the best of our knowledge no literature is currently available reporting its performance on the *ex-situ* catalytic pyrolysis of plastic waste.

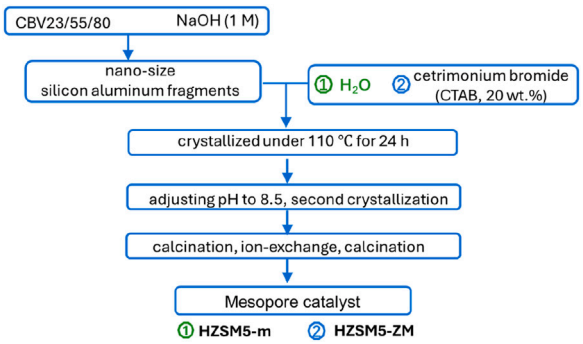


FIGURE 1
Schematic illustration of hierarchical HZSM-5 preparation.

The qualitative and quantitative analysis of pyrolysis products is crucial, which relies on an effective separation system and detector. Two-dimensional gas chromatography (GC × GC) can simultaneously exploit differences in boiling points and polarity of the compounds, enabling the effective separation of aliphatic and aromatic substances at different carbon numbers (Van Geem et al., 2010). These substances are abundant in plastic catalytic pyrolysis, where LO and MA are the main products. Accurate identification and quantification of the formed hydrocarbons by these zeolites provides insight into the involving reaction mechanisms. Furthermore, online analysis offers significant advantages over offline analysis (Van Geem et al., 2010), facilitating better mass balance accuracy and avoiding uncertainty caused by sampling. Therefore, online analysis based on GC × GC coupled with FID/MS detectors is the most ideal system for catalytic pyrolysis of plastic (Dogu et al., 2021). Despite its importance, there is a gap in research utilizing the analytical techniques to study polypropylene (PP) catalytic pyrolysis.

This study investigates the physicochemical properties and catalytic performance of three HZSM-5 zeolites with different $SiO_2/Al_2O_3$ ratios and their modified hierarchical HZSM-5-m and HZSM-5-ZM. The correlation between the catalyst's properties and performance illustrated here determines the extent to which HZSM-5 acidity or pore size promotes its activity toward forming LO and MA, providing valuable insights for developing optimized PP pyrolysis catalysts.

# 2 Experiments and methods

## 2.1 Samples

### 2.1.1 Plastics samples

Polypropylene (PP) was received from Borealis (HE125MO). The sample was initially obtained in pellet form and then downsized using a cutting mill (FRITSCH). The resulting powder was sieved and the particle size <300 μm was collected to mitigate the potential mass and heat transfer limitations.

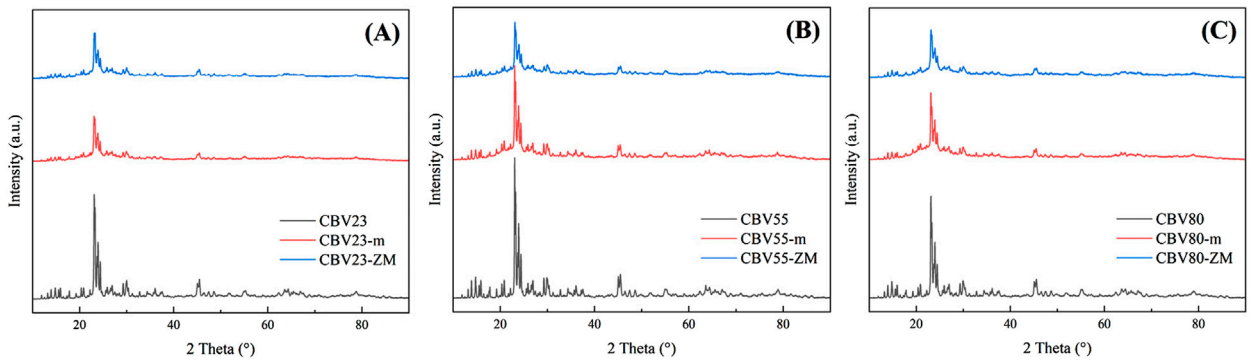


FIGURE 2
XRD patterns of catalysts **(A)** CBV23 series **(B)** CBV55 series **(C)** CBV80 series.

### 2.1.2 Catalyst preparation

Three HZSM-5 catalysts (CBV2314, CBV5524G, and CBV8014) were procured from Zeolyst International. The $SiO_2/Al_2O_3$ molar ratios were 23, 50, and 80, respectively. Before utilization, these catalysts were calcined at 550°C for 4 h in a muffle furnace to obtain the hydrogenated form.

Figure 1 shows the preparative steps followed for hierarchical HZSM-5. To introduce the MCM-41 type mesopore, the catalyst was dissolved in a NaOH/CTAB (Cetyltrimethylammonium bromide, Sigma-Aldrich) solution. First, HZSM-5 was dissolved in 1M NaOH solution (liquid/solid = 10 mL/g) and stirred for 1 h at 60°C. Second, 10wt% CTAB was added (liquid/solid = 20 mL/g) with vigorous stirring for 1 h. The homogenous solution was then transferred into a Teflon-lined autoclave and heated to 110°C for 24 h. The pH was adjusted to 8.5 with 1M HCl and continued to crystallize at 110°C for 24 h. After that, the catalyst was filtered, washed, and dried, followed by the calcination to remove the CTAB template. Finally, ion exchange with $NH_4NO_3$ (1 M) was performed, and the sample was again calcined in a muffle furnace to obtain the hydrogenated catalyst. It should be noted that a neutral pH was ensured after each treatment with basic solutions. A second mesoporous catalyst was prepared, for which 20 mL of deionized water was used as a substitute for a 20 mL CTAB solution, with all other steps remaining identical. The catalyst powder was pelletized, grounded, and sieved to a 100–200 μm particle size.

The parent catalysts are denoted as CBV23, CBV55, and CBV80. The catalysts treated with NaOH are named by adding "m" to the parent catalyst designation, while the catalysts treated with CTAB/NaOH are named by adding "ZM" (HZSM-5/MCM-41). For example, CBV23-m and CBV23-ZM.

## 2.2 Catalyst characterization

### 2.2.1 Pore structure

The pore structure was analyzed by low temperature (−196°C) $N_2$-physisorption using a Tristar II adsorption analyzer (Micromeritics). Approximately 0.1 g of catalyst was weighed for each analysis. Before analysis, all catalysts were degassed at 300°C for 3 h under constant $N_2$ flow. The specific surface area was calculated via the BET approach (Brunauer-Emmett-Teller). The micro, meso, and total pore volume were determined according to the t-plot method, Barrett-Joyner-Halenda (BJH) analysis, and isotherm at $P/P_0 = 0.99$, respectively.

### 2.2.2 Total acid acidity

The total acidity was obtained from $NH_3$-TPD using an Autochem II adsorption analyzer (Micromeritics). A catalyst sample weighing 100 ± 5 mg was placed in the U-shape quartz tube. The sample underwent temperature-programmed desorption in a 4% $NH_3$/He atmosphere, with a heating rate of 10°C $min^{-1}$, reaching the final temperature of 800°C. The concentration and strength of acid sites were measured based on the following Equation 1 (Katada et al., 1997; Niwa et al., 2012).

$$C_g = -\frac{\beta A_0 W}{F}\frac{d\theta}{dT} = \frac{\theta}{1-\theta}\frac{P^0}{RT}\exp\left(-\frac{\Delta H}{RT}\right)\exp\left(\frac{\Delta S}{R}\right) \quad (1)$$

where $\beta$ is the heating rate (10 K $min^{-1}$), $A_0$ is the adsorption capacity (mol $kg^{-1}$), W is the mass of the catalyst (kg), F is the total flow rate (25 mL $min^{-1}$), θ represents the extent of coverage of adsorption sites by ammonia, $P^0$ is the pressure at thermodynamic standard conditions (Pa), ΔH is the enthalpy change (J $mol^{-1}$), and ΔS is the entropy change (J $mol^{-1}$ $K^{-1}$). In this study, ΔS was estimated at 150 J $mol^{-1}$ $K^{-1}$ (Katada et al., 1997). Here, $A_0$ was measured by the integral area under the $NH_3$-TPD curve at high temperature, and ΔH was obtained through curve fitting.

### 2.2.3 Others

The XRD patterns were obtained using a Siemens Kristalloflex D5000 diffractometer with Cu Kα radiation (λ = 0.154 nm). The surface morphology and elemental distribution of the samples were characterized using scanning electron microscopy and energy dispersive X-ray spectroscopy (SEM-EDX, Jeol JSM-5400, INCA).

## 2.3 Catalytic pyrolysis

The micro-pyrolyzer coupled with two-dimensional gas chromatography (GC × GC) was employed to test the catalyst performance (Akin et al., 2023) (Supplementary Material). The micro-pyrolyzer consists of two reactors in series, allowing for separate temperature control. The first reactor is used for thermal

TABLE 1 Relative crystallinity of catalysts (%).

| | CBV23 | CBV55 | CBV80 |
|---|---|---|---|
| HZSM-5 | 100 | 100 | 100 |
| HZSM-5-m | 47 | 68 | 59 |
| HZSM-5-ZM | 50 | 46 | 54 |

pyrolysis and is closely coupled to the second reactor used for catalytic upgrading of pyrolysis vapors. Each test involves loading a 0.4 mg solid sample (described in Section 2.1.1) into a stainless steel cup. The cup was then dropped into the first reactor when the temperature reached 550°C to achieve rapid pyrolysis. At this temperature, complete conversion of polyolefin plastics can be achieved, with no solid residues remaining in the reactor (Akin et al., 2023). Then, the plastic vapors were introduced into the second reactor containing 32 mg catalyst. He carrier gas was maintained at 50 mL $min^{-1}$. The volatiles were injected into the GC × GC analyzer for product identification and quantification. The RTX-1 PONA (50 m, ID = 0.25 mm) and polar BPX-50 (2 m, ID = 0.15 mm) were used as the first and second dimension columns, respectively. The molecular response factor (MRF) was adopted to calculate the product yield, where isobutane was used as the standard (de Saint Laumer et al., 2015). All yields calculated in this study are reported as weight percentages. For catalytic pyrolysis, online analysis allows for a comprehensive analysis of both gas-phase and liquid-phase products. With fewer than 5 uses of the catalyst, the coke adhered to the catalyst surface can be considered negligible (Akin et al., 2024). The carbon balance of the catalytic reaction was more than 95 wt%. The quantified products of catalytic pyrolysis were normalized for relative comparison.

# 3 Results and discussion

## 3.1 Catalyst properties

### 3.1.1 Crystalline structures

Figure 2 shows the XRD patterns of the modified and parent catalysts. The relative crystallinity was calculated based on the peak area in the 2θ range of 22.5°–25°, and assigning crystallinity of the parent catalyst as 100%. Overall, the relative crystallinity of the modified catalysts was ~50% (Table 1). The crystallinity is significantly influenced by NaOH concentration used for catalyst preparation. For instance, treating a catalyst with a $SiO_2/Al_2O_3$ ratio of 55 using 0.2M NaOH resulted in a relative crystallinity of 97% (Sun et al., 2021). Conversely, treating a catalyst with a $SiO_2/Al_2O_3$ ratio of 20 using 3M NaOH resulted in a relative crystallinity of 15% (Tang et al., 2012). Thus, a low NaOH concentration may hinder the recrystallization process, while a high concentration can significantly reduce HZSM-5 crystallinity. In this study, a moderate 1M NaOH concentration was used, allowing the treated catalyst to retain 50% of the HZSM-5 crystalline structure.

### 3.1.2 Textural properties

The results presented in Table 2; Figure 3 show the difference in the pore size distribution and surface area of the parent zeolites with HZSM-5-m and HZSM-5-ZM. The parent catalysts are predominantly microporous, exhibiting $V_{micro}/V_{total}$ ratios of 66%, 55%, and 51% for CBV23, CBV55, and CBV80, respectively. It should be noted that $N_2$-physisorption characterization is limited in measuring the total micropore volume, and these values are underestimated. The $V_{meso}/V_{total}$ ratios for these catalysts are 19%, 24%, and 29%, respectively, indicating the presence of mesopores, particularly in CBV80, which also shows the highest specific surface area and total volume among the parent catalyst.

Mesopore introduction to the parent HZSM-5 significantly changed their pore size and surface area. The $V_{total}$ of CBV23-m, CBV55-m, and CBV80-m are approximately 2.0, 1.9, and 2.3 times larger than their respective HZSM-5 samples. The increased $V_{meso}/V_{total}$ for these samples compared to parent samples is also noticeable, 74%, 79%, and 79%, respectively, while the $V_{micro}/V_{total}$ decreases. Despite the increase in total and mesopore volumes, the $S_{BET}$ for CBV55 and CBV80 decreases after mesopore introduction. This suggests a possible merging of microporous and mesoporous structures, leading to the formation of macropores, as evidenced in Figure 3.

Similarly, the hierarchical core-shell HZSM-5-ZM catalysts have an enhanced total pore volume. CBV23-ZM, CBV55-ZM, and CBV80-ZM have 2.1, 1.7, and 2.2 times more pore volume over their respective parent samples. The $V_{meso}/V_{total}$ ratios for these catalysts, 64%, 67%, and 68%, respectively, indicate the presence of mesopores in high concentrations. More interestingly and in contrast with HZSM-5-m samples, the mesopore size distribution is much better controlled for HZMS-5-ZM resulting in a typical pore size between 2 and 4 nm (Figure 3) while the macropore volume decreased, resulting in a significant increase in $S_{BET}$.

The introduction of mesopores by NaOH usually occurs at the boundaries or defect sites of the catalyst (Groen et al., 2004a), resulting in an expansion of individual pores. CTAB allows the reassembling of these fragments, forming new mesoporous structures (Zhang et al., 2023). In the framework of MFI catalysts, the presence of Al plays a crucial role in preventing Si dissolution. The negatively charged $AlO_4^-$ tetrahedra can hinder the hydrolysis of Si-O-Al bonds (Groen et al., 2004a; Groen et al., 2004b). In contrast, the cleavage of Si-O-Si bonds that lack Al at neighboring sites occurs more easily. It was reported that zeolites with low $SiO_2/Al_2O_3$ ratio (less than 10) are less prone to hydrolysis due to the negatively charged $AlO_4^-$ tetrahedral structures, whereas the zeolite with high $SiO_2/Al_2O_3$ (higher than 25) would lead to excessive and unselective Si dissolution. The Si/Al ratio of catalyst was determined by SEM-EDX (Supplementary Figure S2; Supplementary Table S1). The CBV23 with high Al content showed the smallest change in Si/Al due to the protective effect of $AlO_4^-$ tetrahedra. Overall, the pretreatment had a minor effect on Si/Al ratio of catalyst. In this study, it was observed that the CBV55-m and CBV80-m featured a highly macroporous structure, indicating that the mesopores introduction is uncontrollable for such kind of zeolites. However, under the recrystallization facilitated by CTAB, a well-developed mesopore structure is observed, as evidenced by CBV80-ZM with the sharpest peak in pore size distribution (Figure 3). Conversely, the low $SiO_2/Al_2O_3$ catalyst CBV23 exhibits weaker hydrolysis under 1M NaOH condition, and the recrystallization effect by CTAB is correspondingly weaker. It can be inferred that CBV23 is suitable for mesopore

TABLE 2 Textural properties of the parent and modified HZSM-5, and core-shell HZSM-5-ZM samples.

| Samples | $V_{micro}$[a] [$cm^3\ g^{-1}$] | $V_{meso}$[b] [$cm^3\ g^{-1}$] | $V_{total}$[c] [$cm^3\ g^{-1}$] | BET [$m^2\ g^{-1}$] |
|---|---|---|---|---|
| CBV23 | 0.123 | 0.037 | 0.185 | 329.5 |
| CBV23-m | 0.042 | 0.276 | 0.370 | 342.9 |
| CBV23-ZM | 0.035 | 0.251 | 0.393 | 343.0 |
| CBV55 | 0.115 | 0.049 | 0.207 | 370.1 |
| CBV55-m | 0.061 | 0.313 | 0.395 | 286.5 |
| CBV55-ZM | 0.066 | 0.242 | 0.361 | 456.5 |
| CBV80 | 0.120 | 0.070 | 0.235 | 393.9 |
| CBV80-m | 0.048 | 0.433 | 0.542 | 287.4 |
| CBV80-ZM | 0.052 | 0.357 | 0.524 | 460.7 |

[a]t-plot method.
[b]BJH, adsorption branch for pore width of 20–500 Å
[c]$N_2$ isotherm at $P/P_0 = 0.99$.

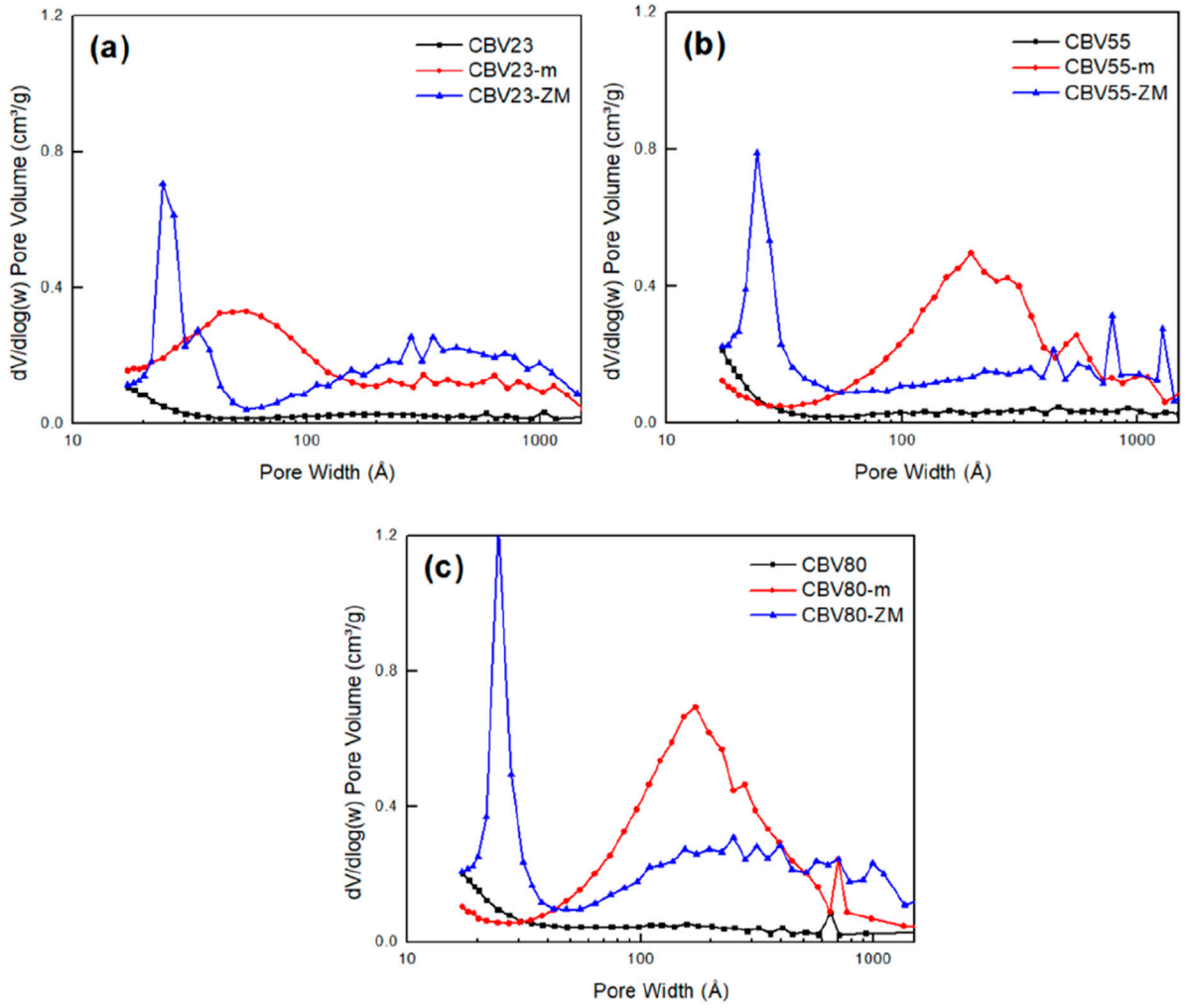


FIGURE 3
BJH analysis of the adsorption branch for parent and hierarchical porous catalysts **(A)** CBV23 **(B)** CBV55 **(C)** CBV80.

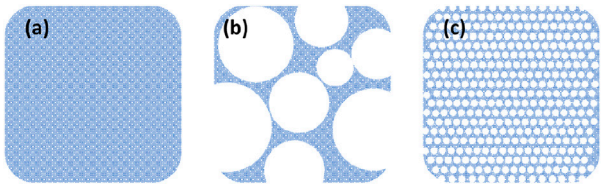


FIGURE 4
Schematic diagrams of the pore structures **(A)** HZSM-5, **(B)** HZSM-5-m, and **(C)** HZSM-5-ZM.

introduction under more concentrated alkali solutions or at higher temperatures.

The engineering of parent zeolites' pore structure and surface characteristics underscores the potential of hierarchical HZSM-5 catalysts to enhance their catalytic performance, particularly for PP pyrolysis involving large and branched molecular reactants. A schematic representative of the obtained engineered structures is shown in Figure 4 based on the $N_2$-physisorption characterization.

### 3.1.3 Catalysts acidity

$NH_3$ Temperature Programmed Desorption ($NH_3$-TPD) results show two distinct peaks for all samples, as illustrated in Supplementary Figure S5. The low-temperature peak (l-peak) at approximately 250°C and high-temperature peak (h-peak) at around 400°C indicate weak and strong acidic sites, respectively. The l-peak is of complex origin, primarily involving weakly bound ammonia, potentially due to hydrogen bonding, and is also influenced by factors such as micropore diffusion and dipole interactions (Katada et al., 1997; Niwa and Katada, 2013). Analysis of the strong acid peak after deconvolution, as discussed in the experimental section, permits a clear interpretation of acid site distributions and their average strengths (Niwa et al., 2012). Strong and weak acid site concentrations increase as the parent catalysts' $SiO_2/Al_2O_3$ mole ratio decreases. Simultaneously, the acid strength distribution becomes slightly narrower as the ratio increases. However, the average enthalpy change ($\Delta H_{avg}$) across these catalysts remains relatively consistent at approximately 133 kJ/mok, suggesting that the strength of acid sites is predominantly dictated by the crystal structure rather than the composition (Katada et al., 1997).

The number and strength of acid sites in HZSM-5-m decreases after introducing mesopores using a NaOH solution. After introducing mesopores, the distribution of acid site strength broadened significantly, indicating more non-homogeneous acid site strengths across the modified samples. When mesopores are introduced using a NaOH/CTAB mixed solution, there is a noticeable enhancement in the concentration of strong acid sites. There is, however, no trend for the strength of the high-temperature acid sites on the HZSM-5-ZM samples compared to their parent catalysts. Specifically, the $\Delta H_{avg}$ of CBV23-ZM decreases from 133.4 to 127.7 kJ $mol^{-1}$, CBV55-ZM shows a minor change, and CBV80-ZM increases from 133.0 to 135.2 kJ $mol^{-1}$ (Table 3). It can be observed that error range for parent catalyst is smaller than the mesoporous HZSM-5. This increased error range in the mesoporous HZSM-5 can be attributed to the easy liberation of trapped $NH_3$ through the mesopores (Liu et al., 2023), thereby contributing to greater variability.

## 3.2 Catalytic pyrolysis

### 3.2.1 GC × GC chromatogram of product distribution

Figure 5 shows the GC × GC chromatogram of the reaction products of the thermal (a) and *ex-situ* catalytic pyrolysis (b) of PP. All relevant products are well-separated by GC × GC. The first GC column separates the hydrocarbon products by their boiling point, while the second column provides separation based on the polarity. An increase in branching leads to a decrease in boiling point, consequently reducing the first dimension retention time (Van Geem et al., 2010). The increase in branching also reduces the second-dimension retention time (von Mühlen et al., 2006). Combining this knowledge and MS spectra, the quantification of paraffins, isoparaffins, olefins, diolefins, naphthenes, and aromatics with altering carbon numbers is achieved. Figure 5A can be broadly divided into the paraffinic and aromatic regions. The paraffinic region at the bottom of the graph includes n-paraffins, isoparaffins, olefins, and naphthenes. The aromatic region at the upper side encompasses monoaromatics, naphthenoaromatics, and diaromatics. It can be found that $C_2$-$C_4$ olefins (LO) are the main products when using the catalyst shown in Figure 5B compared to thermal pyrolysis in Figure 5A. Numerous paraffins, olefins, and naphthene peaks appear with weak LO and MA peaks.

HZSM-5 is characterized by micropores, which measure about 5.5 Å in average size. The normal paraffins are most favored for entering these micropores, followed by monomethyl-substituted paraffins. Other hydrocarbons, such as monocyclic aromatics, also enter these pores, albeit to a lower extent, with dimethyl-substituted paraffins being less preferred (Derouane, 1980). The catalytic reactor feed originates from the PP thermal pyrolysis, which contains a wide range of hydrocarbons. This gas mixture comprises of 11.9% LO; no MA is formed during thermal pyrolysis. The yield of the quantifiable hydrocarbons ranging from $C_1$-$C_{40}$ is 54.7%. According to mass closure calculations, the yield of $C_{21+}$ waxes is approximately 55.1%, and their high molecular size may limit their diffusion into zeolite micropores. It should be mentioned that the pyrolyzed vapor includes branched hydrocarbons, contributing to the molecular complexity and size, as shown for the detectable compounds in Supplementary Table S2. For instance, the minimum kinetic diameter of n-octene is 0.48 nm, which increases to 0.62 nm for iso-octene (Chen W. et al., 2022). Consequently, to enhance molecular diffusion and access to active sites, the pore size of HZSM-5 is often adjusted when dealing with molecules with a large kinetic diameter (Eschenbacher et al., 2022; Jin et al., 2022).

### 3.2.2 Catalytic performance of HZSM-5, HZSM-5-m, and HZSM-5-ZM during PP pyrolysis

Figure 6 shows the product distribution of PP catalytic pyrolysis with different catalysts. These catalysts demonstrate significant selectivity towards LO and MA with a clear distinction in product distribution. As specified in the previous sections, these zeolites differ in $SiO_2/Al_2O_3$ ratio and pore size distribution. CBV23 corresponds to the lowest $SiO_2/Al_2O_3$-ratios and vice versa for CBV80, as specified in section 2.1.2. When comparing $SiO_2/Al_2O_3$ ratios, it can be observed that the catalyst's $SiO_2/Al_2O_3$ ratio follows an opposite trend with a selectivity towards MA,

TABLE 3 Acid sites concentration and their strength determined by $NH_3$ TPD.

| Samples | A[a] [mol $kg^{-1}$] | A[b] [mol $kg^{-1}$] | ΔH[c] [kJ $mol^{-1}$] | $T_{peak}$[d] [°C] |
|---|---|---|---|---|
| CBV23 | 0.382 | 0.619 | 133.4 ± 8.2 | 435 |
| CBV23-m | 0.163 | 0.572 | 128.3 ± 11.1 | 363 |
| CBV23-ZM | 0.143 | 0.763 | 127.4 ± 10.7 | 365 |
| CBV55 | 0.119 | 0.439 | 132.9 ± 5.7 | 400 |
| CBV55-m | 0.113 | 0.328 | 130.9 ± 6.4 | 395 |
| CBV55-ZM | 0.034 | 0.610 | 132.1 ± 13.0 | 393 |
| CBV80 | 0.064 | 0.311 | 133.0 ± 3.6 | 395 |
| CBV80-m | 0.047 | 0.215 | 130.7 ± 5.5 | 375 |
| CBV80-ZM | 0.013 | 0.474 | 135.2 ± 10.8 | 397 |

[a]$NH_3$ desorption amount by low temperature peak (l-peak).
[b]$NH_3$ desorption amount by high temperature peak (h-peak).
[c]desorption enthalpy change for h-peak.
[d]Position for h-peak.

ethylene, and $CH_4$ while correlating positively with the yield of $C_3H_6$, $C_4$-olefins, and nonaromatic $C_5$-$C_{11}$. This trend is consistent across both parent and treated materials. Parent catalysts CBV55 and CBV80 produce comparable LO yields at 78.5% and 79.3%, respectively. However, their ethylene-to-propylene ratio is different. CBV55 produces more ethylene, while CBV80 is more selective to propylene and $C_4$ olefins. CBV23 produces the highest MA, ethylene, and methane yields among the parent catalysts, followed by CBV55 and 80. Specifically, the MA yield using CBV23 is about 31.9%, with benzene and toluene yields reaching 13.9% and 9.5%, respectively. Additionally, the ethylene and methane yields are 32.8% and 7%, respectively.

The relation of product yields with the $SiO_2/Al_2O_3$ ratio of the parent samples can be primarily explained due to their acidity. This is evident as all three parent catalysts with different acid quantities share similar microporous structures, surface area, and $NH_3$-desorption $\Delta H_{avg}$. The change in the $SiO_2/Al_2O_3$ ratio results in a difference in total number of acid sites. Hence, the higher the total number of acid sites, the more pyrolysis vapors can be converted to valuable products, resulting in high methane, MA yields and low $C_5$-$C_{11}$ yields. The methane and MA yields are indicative of the conversion as these hydrocarbons undergo no secondary reactions, and their yields increase monotonously with increasing conversions.

The parallel trends of ethylene and aromatics in Supplementary Figure S7 suggest that the dual-hydrocarbon pool mechanism on HZSM-5 with low $SiO_2/Al_2O_3$ may predominately drive the formation of these chemicals, as this mechanism leads to a high ethylene/propylene ratio (Bjørgen et al., 2007; Sun et al., 2014; Wang et al., 2015; Yarulina et al., 2018). The formed propylene in the mentioned pathway might be even further converted through oligomerization reactions over zeolites with high acidity. HZSM-5 is less active in the oligomerization of ethylene compared to propylene. This is due to the lower stability of its primary carbenium cation compared to the secondary carbenium cations of propylene (Yarlagadda et al., 1990). The olefins oligomerization activation energy was reported to decrease by increasing the HZSM-5 acid concentration, with ethylene requiring an activation energy of approximately 20 kJ/mol more than longer carbon chain olefins (Oliveira et al., 2010). On the other hand, zeolites with weak or low acidity prefer the dimerization-cracking route during 1-pentene catalytic cracking to propylene, a pathway potentially dominantly involved in the PP pyrolysis over CBV80 (Sun et al., 2014).

When investigating the effect of mesopore introduction by treatment with NaOH, there is no uniform trend in product yields across different $SiO_2/Al_2O_3$ ratios. This depicts the high dependency of mesopore introduction on the zeolite acidity and the heterogeneity of the obtained zeolite pores, as argued earlier. The mesoporous zeolites have a lower acidity than their parent catalyst but are more porous, increasing the diffusion rates of reactants and products. These two competing effects compensate for each other partially depending on the $SiO_2/Al_2O_3$ ratio of the zeolite. The more acidic CBV23-m still has a high concentration of acid sites after the alkaline treatment but has superior diffusion rates, resulting in slightly higher ethylene yields and an even more profound increase in propylene yield. In contrast, with CBV55-m, the total acidity (0.558 mol $kg^{-1}$) is much lower than that of CBV23-m (0.735 mol $kg^{-1}$), resulting in much lower ethylene and propylene yields, while the yield of $C_5$-$C_{11}$ nonaromatics increased. This indicates that the loss in acidity by introducing mesopores cannot be compensated by the enhanced accessibility of the active sites. Lastly, CBV80-m has slightly higher ethylene, propylene, and MA yields, while the fraction of butenes and $C_5$-$C_{11}$ dropped compared to its parent catalyst. Even though CBV80-m has a low concentration of acid sites (0.262 mol $kg^{-1}$) it has the highest pore volume of all zeolites studied in this work (0.542 $cm^3$ $g^{-1}$). As a result, the increased yields in light olefins for CBV80-m can be explained by the elevated diffusion rates.

Lastly, the combined NaOH/CTAB treatment for producing hierarchical zeolites had a profound increase in propylene yield compared to their parent zeolites independent of the parent catalyst's acidity. While only small deviations in ethylene, MA, and $C_5$-$C_{11}$ yields were observed, the differences were most profound for propylene and $C_4$ olefins. The hierarchical zeolites have a slightly lower acidity than their parent catalysts but compensate for this with much better diffusional properties and

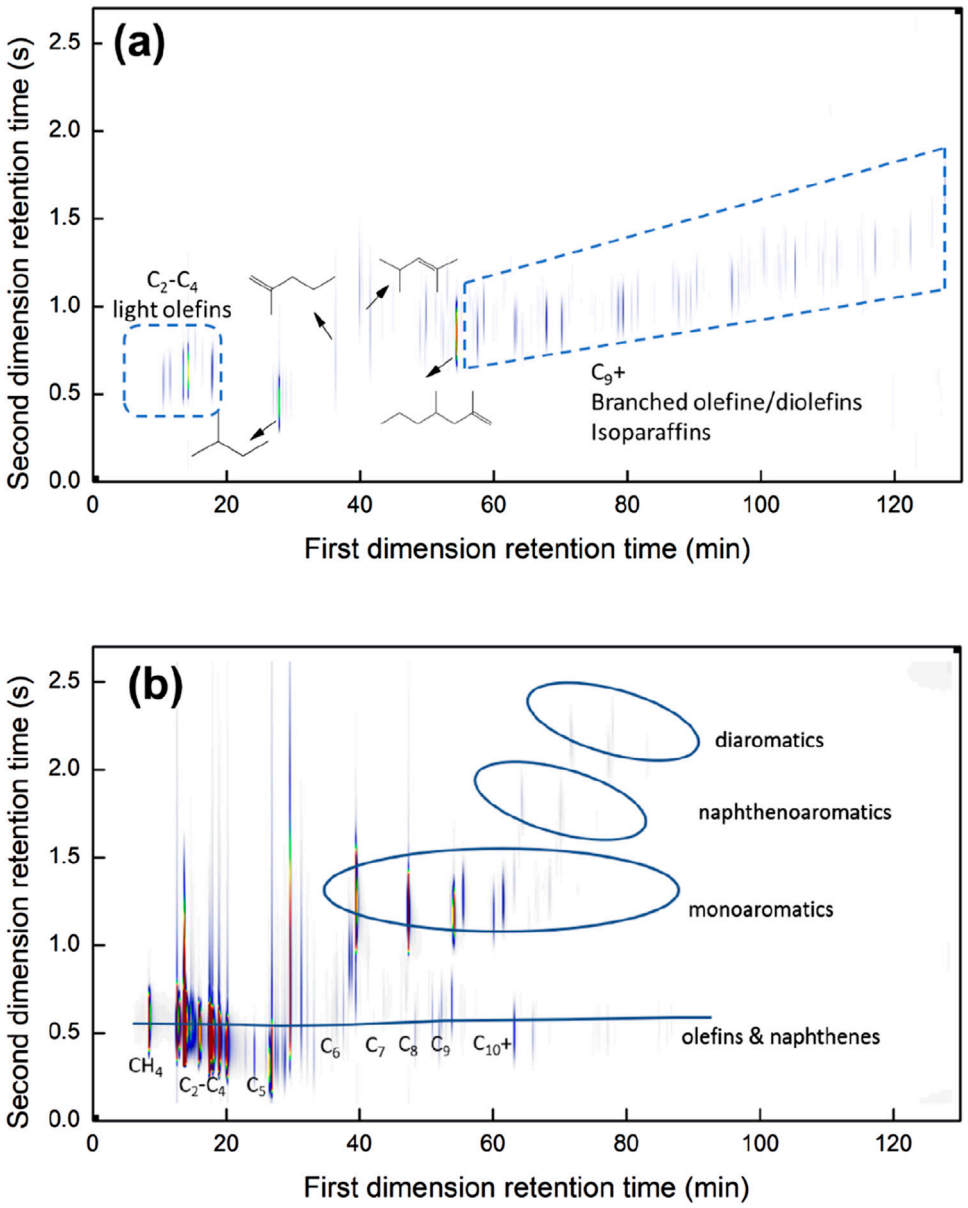


FIGURE 5
On-line GC × GC-FID chromatograph of PP **(A)** thermal pyrolysis and **(B)** catalytic pyrolysis using CBV55.

a narrow mesopore distribution with an average pore size of 30 Å. As a result, the branched propylene oligomers diffuse much easier in the hierarchical zeolites, resulting in an increased propylene yield, while the acidity is maintained sufficiently to maintain proper conversions. The maximum propylene yield, approximately 40%, is achieved with CBV55-ZM and CBV80-ZM. This is accompanied by yields of 77% for LO and 15% for MA, culminating in a combined yield of MA and LO of 92%.

## 3.3 Dependency of product yields on zeolite acidity

The catalytic performances showed that the product distribution changes when the modifications alter the catalyst's acidity and pore structure. Figure 7 shows the relation of the obtained product yields with weak, strong, and total acid sites. This provides further insights into how product yields depend on zeolite acidity. It should be noted that most product yields correlate very well with the zeolite acidity, indicating the importance of this parameter in zeolite design. As discussed previously, a high MA yield accompanies a high ethylene yield (Supplementary Figure S7). Similarly, ethylene and MA yields follow nearly the same patterns when varying the catalyst properties, as shown in Figure 7. These compounds positively correlate with the total catalyst acidity.

On the contrary, propylene yield correlates with weak acid sites negatively while nearly no correlation is obtained for the strong and total acid site concentration. The presence of weak acid sites facilitates isomerization reactions of hydrocarbons upon catalytic pyrolysis. These isomerization reactions result in a much more

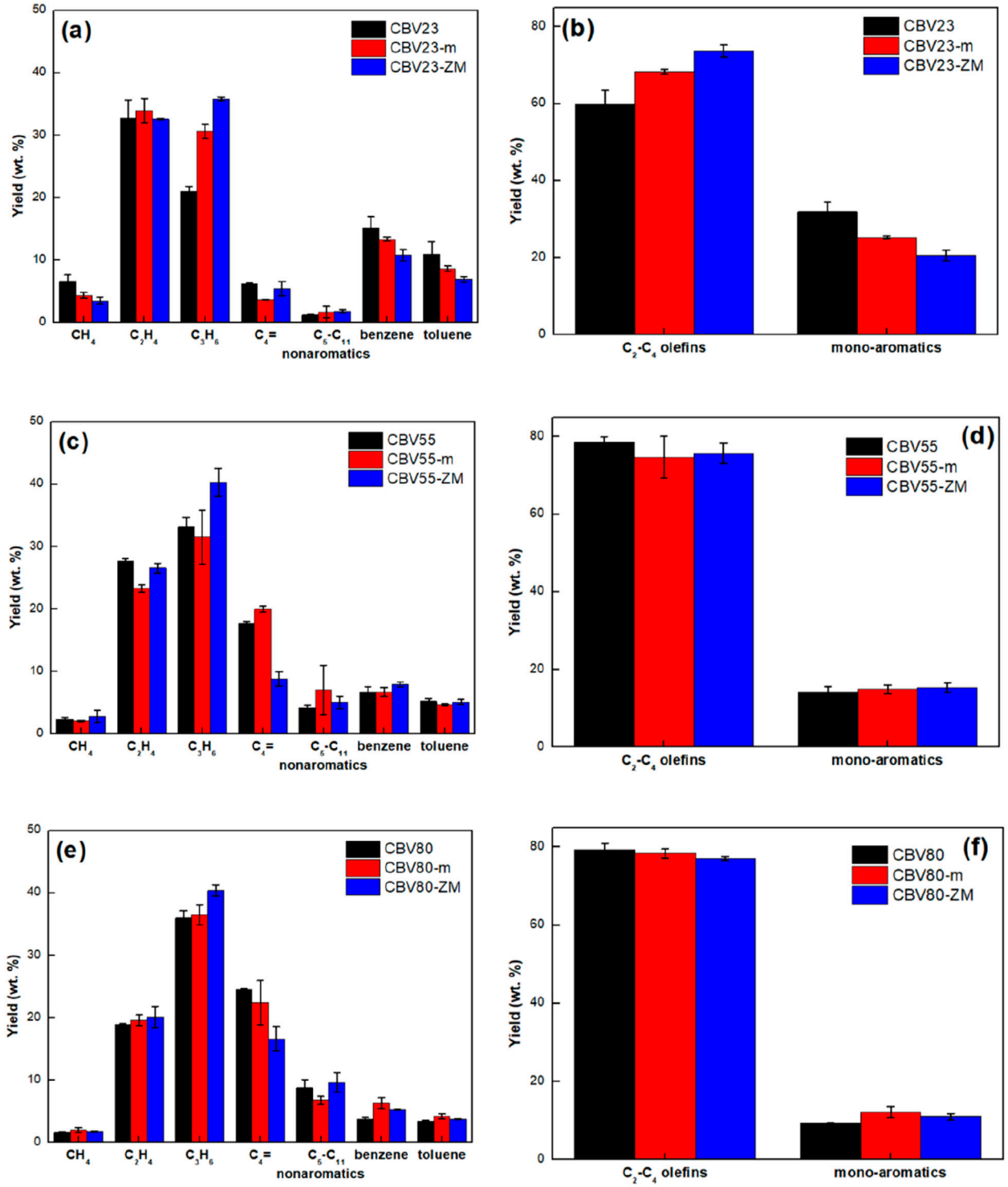


FIGURE 6
Product distribution for PP catalytic pyrolysis at a catalytic temperature of 550°C, 50 mL He/min, and catalyst/feed ratio of 80 using different catalysts **(A, B)** CBV23, **(C, D)** CBV55 and **(E, F)** CBV80.

complex product distribution and decrease the yield of the main product, propylene. As a result, the propylene yield strongly depends on the concentration of weak acid sites.

$C_4$= possesses a negative linear relation with strong acid sites, while a plateau in their yields is reached by varying the catalyst surface area at 400 $m^2g^{-1}$ (Supplementary Figure S10). It can be concluded that there is a tradeoff between propylene and C4 olefin yields versus ethylene and MA yields, and a balance of catalyst properties is required for maximized product yield. These results enable generalizing some of the experimental findings across the

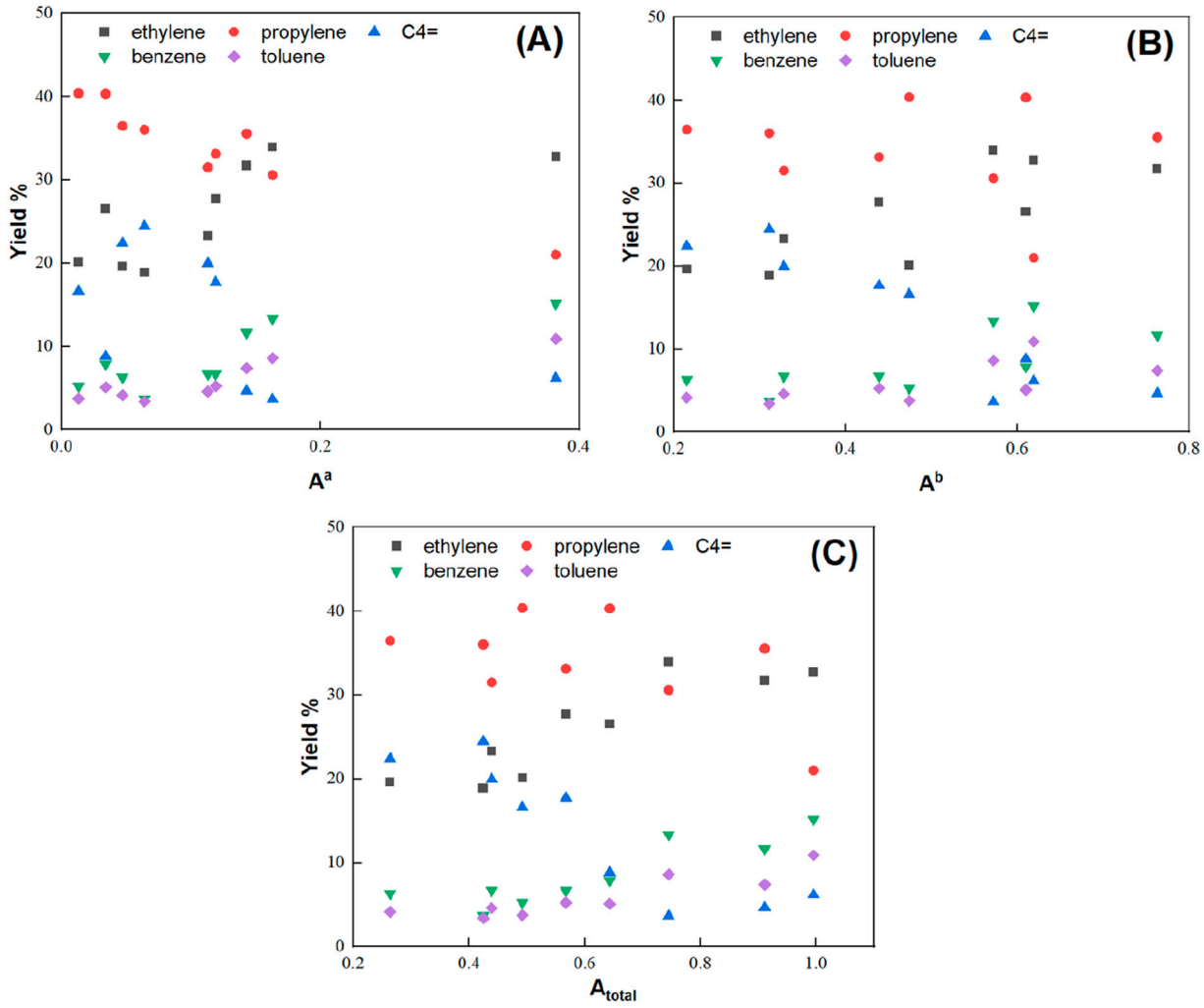


FIGURE 7
Effect of catalyst acidity, **(A)** weak acid sites, **(B)** strong acid sites, **(C)** total acid sites, on product yields using HZSM-5, HZSM-5-m, and HZSM-5-ZM.

nine different HZSM-5 catalysts despite their varying physiochemical properties.

The impact of HZSM-5 properties on product distribution is a subject of ongoing debate in the literature. Dai et al. studied hierarchical HZSM-5, treated by TPAOH, for the catalytic cracking of HDPE vapors (Dai et al., 2022; Dai et al., 2023). The modification with mesopores enhanced molecular transport, as evidenced by increased uptake of 2,2-dimethylbutane and large dye molecules. Investigating the relation between Brønsted acid surface density (BAS/$S_{BET}$) and aromatics yield revealed a non-linear interaction characterized by a maximum aromatic yield at middle-range acid density (0.5 μmol/$m^2$). They also showed that Brønsted acid site surface density plays a more important role in aromatics selectivity and catalyst lifetime than mesoporosity. Further research by Guo et al. showed that employing HZSM-5/MCM-41 catalysts for the catalytic pyrolysis of cellulose led to a remarkable yield of 89 wt% for BTEX (benzene, toluene, ethylbenzene, and xylene) (Guo et al., 2022). They suggested that catalyst acidity and pore size synergistically influence the catalytic performance. Marcilla et al. (2006) employed TGA to investigate the catalytic pyrolysis of PP and LDPE. It was observed that when using HZSM5, the reactivity of LDPE was enhanced more significantly compared to PP, whereas when using MCM-41, the reactivity of PP showed a greater enhancement than LDPE. They attributed this phenomenon to the larger pore size of MCM-41, allowing for a more extensive catalytic effect on the tertiary carbon atoms.

## 3.4 Mechanistic insights into mesopore modifications

This section presents the reaction mechanism of the *ex-situ* catalytic pyrolysis of PP to provide additional insight into the obtained results and the importance and effect of mesoporous modifications. Figure 8 shows an illustrative mechanism indicating the effect of various catalyst properties and the main products formed by the catalytic pyrolysis of PP. The PP vapors contain many heavy hydrocarbons, with the share of $C_{10}$+ hydrocarbons exceeding 63.8 wt% (Supplementary Table S2). It should be noted that the PP vapors contain a pretty high

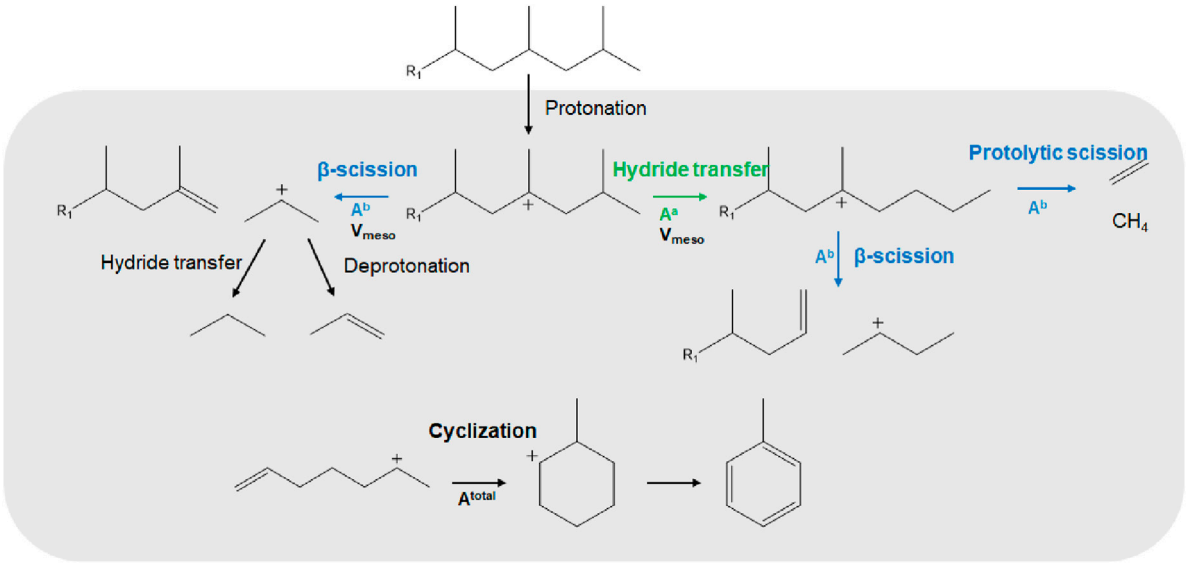


FIGURE 8
*Ex-situ* catalytic pyrolysis mechanism of polypropylene (grey area depicting adsorbed species).

concentration of olefins, and the cracking of the olefins is hundreds of times faster than that of alkanes (Williams et al., 1999).

The main active sites of zeolite catalysts are Brønsted acid sites (BAS), provided by the proton attached to the Si-O-Al bridging linkages. The BAS sites are distributed on the zeolite, especially the external surface (Wang et al., 2023). The large molecular hydrocarbons in PP vapors undergo the preliminary cracking on the external surface and pore mouth of zeolite, so that further depolymerization can occur within the micropore. The coke formation on the outer surface and pore mouth strongly affects the PP catalytic pyrolysis (Akin et al., 2024). Long-chain hydrocarbons form carbocation intermediates at BAS through protonation (Zhao et al., 2023). Subsequently, these carbenium ions undergo either cleavage of carbon-carbon bonds at the β-position, forming shorter-chain hydrocarbons and carbocations, or isomerization reactions. The β-scission pathway is the primary reaction of the catalytic pyrolysis of plastic with HZSM-5, leading to propylene production (Negelein et al., 1998). As shown in Figure 8, propylene is predominantly produced by the β-scission of branched hydrocarbons. However, the diffusion of these branched hydrocarbons is limited by the size of the reactants and the untreated HZSM-5 micropores. That is why introducing mesoporosity while maintaining strong acid sites significantly enhances the propylene yields, as evidenced by the yields of the HZSM-5-ZM in Figure 6. This is consistent with the reported relation between strong acid sites and the zeolite pore structures with propylene yield (Haag et al., 1991; Buchanan et al., 1996; Negelein et al., 1998).

On the other hand, weak acid sites favor isomerization reactions such as hydride- and methyl-shifts and protonated cyclopropane isomerization (Haag et al., 1991; Buchanan et al., 1996; Weitkamp, 2012). The produced carbenium ions by β-scission then predominantly undergo deprotonation, forming olefins, or intermolecular hydride transfer, forming paraffins (Rahimi and Karimzadeh, 2011). The latter is typically suppressed in MFI topologies. This set of reactions forms non-branched products such as butenes, whose yield negatively correlates with strong acid sites, as shown in Figure 6. Therefore, increasing the strong-to-weak acid ratio can limit the reaction pathways starting from isomerization.

Ethylene, methane, and MA yields were most strongly influenced by the total acidity and, to a lesser extent, the pore distribution. This is because the smaller molecules produced by thermal and catalytic pyrolysis can diffuse into the micropores at medium conversions, generating the MA through the Diels-Alder or cyclization reactions, as presented at the bottom of Figure 8. Simultaneously, methane, ethane, or ethylene can be formed through protolytic or alpha-scission (Uslamin et al., 2020). Higher total acidity enhances their respective yields, making mesoporous zeolites and the high $SiO_2/Al_2O_3$ ratio less favorable for their formation (Figures 6, 7).

In summary, the product yields of the *ex-situ* catalytic pyrolysis of PP are mainly dependent on the catalyst acidity and porosity. Ethylene, methane, and MA yields were most strongly influenced by the acidity and, to a lesser extent, the pore distribution. Higher acidity enhances the respective yields, making mesoporous or hierarchical MFI zeolites less favorable than their corresponding parent zeolite. On the other hand, propylene and butene yields were altered both by the acidity and pore distribution. Propylene is obtained by the β-scission of branched hydrocarbons, which diffuse difficultly through the MFI framework. Therefore, increasing the pore sizes while maintaining strong acid sites favors propylene production. Moreover, weak acid sites were found to be severely detrimental to the propylene yields as these enhance isomerization reactions and increase butene yields. Hence, the hierarchical CBV-80-ZM produced by NaOH/CTAB treatment is an excellent catalyst for enhancing propylene yield during catalytic pyrolysis of polypropylene. This is due to its combination of physiochemical properties: (I) increased pore sizes and enhanced diffusion rates, (II) preserved and increased number of strong acid

sites, and (III) decreased number of weak acid sites, compared to CBV-80 and zeolites with lower $SiO_2/Al_2O_3$ ratios.

Additionally, it is also important to specifically analyze the Brønsted acid sites (BAS) and Lewis acid sites (LAS). Studies on the catalytic cracking of model compounds suggest that to enhance propylene selectivity, a catalyst with a moderate amount of BAS should be chosen to prevent excessive hydrogen transfer and aromatization reactions (Sun et al., 2021; Chen J. et al., 2022; Xiao et al., 2022). A lower BAS/LAS ratio is also preferred to promote bimolecular reactions and enhance propylene selectivity (Liu et al., 2024). A catalyst with these characteristics, such as a phosphorus-modified and steam-treated catalyst used for the catalytic pyrolysis of plastics and plastic-derived oils, can significantly increase the yield of light olefins in the products (Eschenbacher et al., 2022; Tran et al., 2024). It is important to characterize acid sites using FTIR with adsorbed pyridine and this can be considered in future studies.

## 4 Conclusion

This study aimed to modify the physicochemical properties of CBV23, CBV55, and CBV80 zeolites to improve their performance in the catalytic pyrolysis of PP. Specifically, it investigated the effects of NaOH and NaOH/CTAB treatments on these catalysts to optimize their acidity, surface area, and mesopore size. The combined NaOH/CTAB treatment preserves and enhances the concentration of strong acid sites and achieves a higher surface area with a more uniform mesopore distribution than the NaOH method. In addition, the effectiveness of the alkaline treatment was found to be dependent on $SiO_2/Al_2O_3$ ratio. The hierarchical CBV80-ZM catalyst achieved the highest propylene yield at 41 wt% and a total light olefins and mono-aromatics yield of 92 wt%. The property-performance correlation analysis highlighted the primary influence of catalyst acidity on the product yields. Ethylene and MA yields are positively correlated with the total acid sites, indicating that higher acidity promotes the formation of these products. Conversely, the propylene yield negatively correlated with weak acid sites and required mesoporosity to enhance the diffusion rates. These findings emphasize the importance of tailoring catalyst properties to achieve specific product distributions during PP pyrolysis. While hierarchical HZSM-5 has shown to enhance the propylene yield, future research should focus on optimizing the catalyst properties to improve propylene yields, by further reducing the number of weak acid sites and improving the pore distribution. In this way, more valuable propylene can be obtained to close the loop for polypropylene waste.

## Data availability statement

The original contributions presented in the study are included in the article/Supplementary Material, further inquiries can be directed to the corresponding author.

## Author contributions

QH: Writing–review and editing, Investigation, Methodology, Writing–original draft, Conceptualization, Visualization. OA: Methodology, Writing–review and editing, Conceptualization, Formal Analysis. YU: Writing–review and editing, Data curation, Formal Analysis. PY: Data curation, Formal Analysis, Writing–review and editing. LL: Writing–review and editing, Investigation. RV: Writing–review and editing, Formal Analysis. KV: Writing–review and editing, Funding acquisition, Project administration, Supervision.

## Funding

The author(s) declare that financial support was received for the research, authorship, and/or publication of this article. We gratefully acknowledge the financial support of the Flemish Government and Flanders Innovation and Entrepreneurship (VLAIO) through the Moonshot project PREFER (HBC.2020.2609) and Catalisti clusterSBO project WATCH (HBC.2019.0001). The research leading to these results has also received funding from the European Research Council (ERC) under the European Union's Horizon 2020 Programme (P8/2007–2013)/ERC grant agreement no. 818607 (OPTIMA). Qing He acknowledges a personal grant from the Research Fund of Ghent University (BOF; 01P04022). Yannick Ureel acknowledges financial support from the Fund for Scientific Research Flanders (FWO Flanders) through the doctoral fellowship grant 1185822N.

## Conflict of interest

The authors declare that the research was conducted in the absence of any commercial or financial relationships that could be construed as a potential conflict of interest.

## Publisher's note



## Supplementary material

The Supplementary Material for this article can be found online at: https://www.frontiersin.org/articles/10.3389/fceng.2024.1439400/full#supplementary-material

# References


Abbas-Abadi, M. S., Ureel, Y., Eschenbacher, A., Vermeire, F. H., Varghese, R. J., Oenema, J., et al. (2023). Challenges and opportunities of light olefin production via thermal and catalytic pyrolysis of end-of-life polyolefins: towards full recyclability. *Prog. Energy Combust. Sci.* 96, 101046. doi:10.1016/j.pecs.2022.101046

Akin, O., He, Q., Yazdani, P., Wang, Y., Varghese, R. J., Poelman, H., et al. (2024). Tailored HZSM-5 catalyst modification via phosphorus impregnation and mesopore introduction for selective catalytic conversion of polypropylene into light olefins. *J. Anal. Appl. Pyrolysis* 181, 106592. doi:10.1016/j.jaap.2024.106592

Akin, O., Varghese, R. J., Eschenbacher, A., Oenema, J., Abbas-Abadi, M. S., Stefanidis, G. D., et al. (2023). Chemical recycling of plastic waste to monomers: effect of catalyst contact time, acidity and pore size on olefin recovery in *ex-situ* catalytic pyrolysis of polyolefin waste. *J. Anal. Appl. Pyrolysis* 172, 106036. doi:10.1016/j.jaap.2023.106036

Aristizábal-Lanza, L., Mankar, S. V., Tullberg, C., Zhang, B., and Linares-Pastén, J. A. (2022). Comparison of the enzymatic depolymerization of polyethylene terephthalate and AkestraTM using Humicola insolens cutinase. *Front. Chem. Eng.* 4, 1048744. doi:10.3389/fceng.2022.1048744

Bjørgen, M., Svelle, S., Joensen, F., Nerlov, J., Kolboe, S., Bonino, F., et al. (2007). Conversion of methanol to hydrocarbons over zeolite H-ZSM-5: on the origin of the olefinic species. *J. Catal.* 249 (2), 195–207. doi:10.1016/j.jcat.2007.04.006

Buchanan, J. S., Santiesteban, J. G., and Haag, W. O. (1996). Mechanistic considerations in acid-catalyzed cracking of olefins. *J. Catal.* 158 (1), 279–287. doi:10.1006/jcat.1996.0027

Chen, J., Yan, H., Gong, H., Zhang, H., Zhou, Y., Gao, C., et al. (2022a). Tetrahedrally coordinated W(VI) species induced Lewis acid for stable catalytic cracking of 1-hexene to propene. *Chem. Eng. J.* 448, 137504. doi:10.1016/j.cej.2022.137504

Chen, W., Zhao, H., Xue, Y., and Chang, X. (2022b). Adsorption effect and adsorption mechanism of high content zeolite ceramsite on asphalt VOCs. *Materials* 15 (17), 6100. doi:10.3390/ma15176100

Dai, L., Zhao, H., Zhou, N., Cobb, K., Chen, P., Cheng, Y., et al. (2023). Catalytic microwave-assisted pyrolysis of plastic waste to produce naphtha for a circular economy. *Resour. Conservation Recycl.* 198, 107154. doi:10.1016/j.resconrec.2023.107154

Dai, L., Zhou, N., Cobb, K., Chen, P., Wang, Y., Liu, Y., et al. (2022). Insights into structure–performance relationship in the catalytic cracking of high density polyethylene. *Appl. Catal. B Environ.* 318, 121835. doi:10.1016/j.apcatb.2022.121835

Dapsens, P. Y., Mondelli, C., and Perez-Ramirez, J. (2015). Design of Lewis-acid centres in zeolitic matrices for the conversion of renewables. *Chem. Soc. Rev.* 44 (20), 7025–7043. doi:10.1039/c5cs00028a

Derouane, E. G. (1980). "New aspects of molecular shape-selectivity: catalysis by zeolite ZSM - 5," in *Studies in surface science and catalysis* (Amsterdam: Elsevier), 5–18.

de Saint Laumer, J. Y., Leocata, S., Tissot, E., Baroux, L., Kampf, D. M., Merle, P., et al. (2015). Prediction of response factors for gas chromatography with flame ionization detection: algorithm improvement, extension to silylated compounds, and application to the quantification of metabolites. *J. Sep. Sci.* 38 (18), 3209–3217. doi:10.1002/jssc.201500106

Dogu, O., Pelucchi, M., Van de Vijver, R., Van Steenberge, P. H. M., D'Hooge, D. R., Cuoci, A., et al. (2021). The chemistry of chemical recycling of solid plastic waste via pyrolysis and gasification: state-of-the-art, challenges, and future directions. *Prog. Energy Combust. Sci.* 84, 100901. doi:10.1016/j.pecs.2020.100901

Eschenbacher, A., Goodarzi, F., Varghese, R. J., Enemark-Rasmussen, K., Kegnæs, S., Abbas-Abadi, M. S., et al. (2021). Boron-modified mesoporous ZSM-5 for the conversion of pyrolysis vapors from LDPE and mixed polyolefins: maximizing the C2–C4 olefin yield with minimal carbon footprint. *ACS Sustain. Chem. and Eng.* 9 (43), 14618–14630. doi:10.1021/acssuschemeng.1c06098

Eschenbacher, A., Varghese, R. J., Delikonstantis, E., Mynko, O., Goodarzi, F., Enemark-Rasmussen, K., et al. (2022). Highly selective conversion of mixed polyolefins to valuable base chemicals using phosphorus-modified and steam-treated mesoporous HZSM-5 zeolite with minimal carbon footprint. *Appl. Catal. B Environ.* 309, 121251. doi:10.1016/j.apcatb.2022.121251

García, R. A., Serrano, D. P., and Otero, D. (2005). Catalytic cracking of HDPE over hybrid zeolitic–mesoporous materials. *J. Anal. Appl. Pyrolysis* 74 (1), 379–386. doi:10.1016/j.jaap.2004.11.002

Groen, J. C., Jansen, J. C., Moulijn, J. A., and Pérez-Ramírez, J. (2004a). Optimal aluminum-assisted mesoporosity development in MFI zeolites by desilication. *J. Phys. Chem. B* 108 (35), 13062–13065. doi:10.1021/jp047194f

Groen, J. C., Peffer, L. A. A., Moulijn, J. A., Pérez, R. x., and rez, J. (2004b). On the introduction of intracrystalline mesoporosity in zeolites upon desilication in alkaline medium. *Microporous Mesoporous Mater.* 69 (1), 29–34. doi:10.1016/j.micromeso.2004.01.002

Guo, T., Ma, X., Li, Z., Zheng, L., Fan, Q., Ding, X., et al. (2022). Enhancing high selectivity production of light aromatics from *in-situ* catalytic upgrading of cellulose pyrolysis vapors by regulating hierarchical core-shell ZSM-5@MCM-41. *J. Anal. Appl. Pyrolysis* 168, 105774. doi:10.1016/j.jaap.2022.105774

Haag, W. O., Dessau, R. M., and Lago, R. M. (1991). "Kinetics and mechanism of paraffin cracking with zeolite catalysts," in *Studies in surface science and catalysis* (Amsterdam: Elsevier Seientific Publishing Company), 255–265.

Hussain, I., Ganiyu, S. A., Alasiri, H., and Alhooshani, K. (2022). A state-of-the-art review on waste plastics-derived aviation fuel: unveiling the heterogeneous catalytic systems and techno-economy feasibility of catalytic pyrolysis. *Energy Convers. Manag.* 274, 116433. doi:10.1016/j.enconman.2022.116433

Jin, R., Ma, K., Xu, S., Wei, Y., Song, L., Li, Z., et al. (2022). Effect of acid distribution and pore structure of ZSM-5 on catalytic performance. *React. Chem. and Eng.* 7 (10), 2152–2162. doi:10.1039/d2re00065b

Katada, N., Igi, H., Kim, J.-H., and Miki Niwa, (1997). Determination of the acidic properties of zeolite by theoretical analysis of temperature-programmed desorption of ammonia based on adsorption equilibrium. *J. Phys. Chem. B* 101 (31), 5969–5977. doi:10.1021/jp9639152

Li, X., Ge, S., Shao, S., Lv, Z., Xiang, X., and Cai, Y. (2021). Promoted production of hydrocarbons in the catalytic pyrolysis of rape straw over composite HZSM-5@MCM-41 catalysts. *J. Anal. Appl. Pyrolysis* 157, 105067. doi:10.1016/j.jaap.2021.105067

Liu, K., Ramirez, A., Zhang, X., Caglayan, M., Gong, X., Gascon, J., et al. (2023). Interplay between particle size and hierarchy of zeolite ZSM-5 during the $CO_2$-to-aromatics process. *ChemSusChem* 16 (19), e202300608. doi:10.1002/cssc.202300608

Liu, Q., Yang, Z., Chen, Z., Xiao, P., Ge, Y., Piao, Y., et al. (2024). Hydrothermally Ce modified HZSM-5 zeolite enhancing its strong acidity and Brønsted/Lewis acid ratio: stably boosting ethylene/propylene ratio for cracking n-heptane. *Fuel* 368, 131632. doi:10.1016/j.fuel.2024.131632

Marcilla, A., Gómez-Siurana, A., and Berenguer, D. (2006). Study of the influence of the characteristics of different acid solids in the catalytic pyrolysis of different polymers. *Appl. Catal. A General* 301 (2), 222–231. doi:10.1016/j.apcata.2005.12.018

Matsuura, S., Hashimoto, T., and Ishihara, A. (2022). Catalytic cracking of low-density polyethylene over zeolite-containing hierarchical two-layered catalyst with different mesopore size using Curie point pyrolyzer. *Fuel Process. Technol.* 227, 107106. doi:10.1016/j.fuproc.2021.107106

Na, K., Choi, M., and Ryoo, R. (2013). Recent advances in the synthesis of hierarchically nanoporous zeolites. *Microporous Mesoporous Mater.* 166, 3–19. doi:10.1016/j.micromeso.2012.03.054

Negelein, D. L., Lin, R., and White, R. L. (1998). Effects of catalyst acidity and HZSM-5 channel volume on polypropylene cracking. *J. Appl. Polym. Sci.* 67 (2), 341–348. doi:10.1002/(SICI)1097-4628(19980110)67:2<341::AID-APP15>3.0.CO;2-0

Niwa, M., and Katada, N. (2013). New method for the temperature- programmed desorption (TPD) of ammonia experiment for characterization of zeolite acidity: a review. *Chem. Rec.* 13 (5), 432–455. doi:10.1002/tcr.201300009

Niwa, M., Sota, S., and Katada, N. (2012). Strong Brønsted acid site in HZSM-5 created by mild steaming. *Catal. Today* 185 (1), 17–24. doi:10.1016/j.cattod.2011.09.028

Oliveira, P., Borges, P., Pinto, R. R., Lemos, M. A. N. D. A., Lemos, F., Védrine, J. C., et al. (2010). Light olefin transformation over ZSM-5 zeolites with different acid strengths – a kinetic model. *Appl. Catal. A General* 384 (1-2), 177–185. doi:10.1016/j.apcata.2010.06.032

Qian, M., Lei, H., Villota, E., Zhao, Y., Huo, E., Wang, C., et al. (2021). Enhanced production of renewable aromatic hydrocarbons for jet-fuel from softwood biomass and plastic waste using hierarchical ZSM-5 modified with lignin-assisted re-assembly. *Energy Convers. Manag.* 236, 114020. doi:10.1016/j.enconman.2021.114020

Rahimi, N., and Karimzadeh, R. (2011). Catalytic cracking of hydrocarbons over modified ZSM-5 zeolites to produce light olefins: a review. *Appl. Catal. A General* 398 (1-2), 1–17. doi:10.1016/j.apcata.2011.03.009

Shen, Z., Ma, C., Wang, D., He, J., Sun, H., Zhu, Z., et al. (2021). Shape-selective alkylation of benzene with ethylene over a core–shell ZSM-5@MCM-41 composite material. *Chin. J. Chem. Eng.* 37, 64–71. doi:10.1016/j.cjche.2021.05.030

Sun, H., Cao, L., Zhang, Y., Zhao, L., Gao, J., and Xu, C. (2021). Effect of catalyst acidity and reaction temperature on hexene cracking reaction to produce propylene. *Energy and Fuels* 35 (4), 3295–3306. doi:10.1021/acs.energyfuels.0c03544

Sun, X., Mueller, S., Liu, Y., Shi, H., Haller, G. L., Sanchez-Sanchez, M., et al. (2014). On reaction pathways in the conversion of methanol to hydrocarbons on HZSM-5. *J. Catal.* 317, 185–197. doi:10.1016/j.jcat.2014.06.017

Tang, Q., Xu, H., Zheng, Y., Wang, J., Li, H., and Zhang, J. (2012). Catalytic dehydration of methanol to dimethyl ether over micro–mesoporous ZSM-5/MCM-41 composite molecular sieves. *Appl. Catal. A General* 413-414, 36–42. doi:10.1016/j.apcata.2011.10.039

Tran, X. T., Mun, D. H., Shin, J., Kang, N. Y., Park, D. S., Park, Y.-K., et al. (2024). Maximizing light olefin production via one-pot catalytic cracking of crude waste plastic pyrolysis oil. *Fuel* 361, 130703. doi:10.1016/j.fuel.2023.130703

Uslamin, E. A., Saito, H., Kosinov, N., Pidko, E., Sekine, Y., and Hensen, E. J. M. (2020). Aromatization of ethylene over zeolite-based catalysts. *Catal. Sci. and Technol.* 10 (9), 2774–2785. doi:10.1039/c9cy02108f

Van Geem, K. M., Pyl, S. P., Reyniers, M. F., Vercammen, J., Beens, J., and Marin, G. B. (2010). On-line analysis of complex hydrocarbon mixtures using comprehensive two-dimensional gas chromatography. *J. Chromatogr. A* 1217 (43), 6623–6633. doi:10.1016/j.chroma.2010.04.006

von Mühlen, C., Zini, C. A., Caramão, E. B., and Marriott, P. J. (2006). Applications of comprehensive two-dimensional gas chromatography to the characterization of petrochemical and related samples. *J. Chromatogr. A* 1105 (1), 39–50. doi:10.1016/j.chroma.2005.09.036

Wang, S., Chen, Y., Wei, Z., Qin, Z., Ma, H., Dong, M., et al. (2015). Polymethylbenzene or alkene cycle? Theoretical study on their contribution to the process of methanol to olefins over H-ZSM-5 zeolite. *J. Phys. Chem. C* 119 (51), 28482–28498. doi:10.1021/acs.jpcc.5b10299

Wang, T., Feng, X., Lin, D., Li, Y., Shang, J., Zhang, J., et al. (2024). Regulating framework aluminum location towards boosted light olefins generation in *ex-situ* catalytic pyrolysis of low-density polyethylene. *Chem. Eng. J.* 485, 149737. doi:10.1016/j.cej.2024.149737

Wang, W., Zhang, F., Chang, P., Luo, X., Miao, K., and Feng, G. (2022). One-step microwave synthesis of micron-sized ZSM-5/MCM-41 hierarchical porous materials for phenol hydroxyl alkylation. *Inorg. Chem. Commun.* 143, 109738. doi:10.1016/j.inoche.2022.109738

Wang, Y.-l., Zhang, X.-c., Zhan, G.-g., Wang, M.-m., Li, W.-Q., and Cao, J.-p. (2023). Comparing the effects of hollow structure and mesoporous structure of ZSM-5 zeolites on catalytic performances in methanol aromatization. *Mol. Catal.* 540, 113044. doi:10.1016/j.mcat.2023.113044

Weitkamp, J. (2012). Catalytic hydrocracking—mechanisms and versatility of the process. *ChemCatChem* 4 (3), 292–306. doi:10.1002/cctc.201100315

Williams, B. A., Babitz, S. M., Miller, J. T., Snurr, R. Q., and Kung, H. H. (1999). The roles of acid strength and pore diffusion in the enhanced cracking activity of steamed Y zeolites. *Appl. Catal. A General* 177 (2), 161–175. doi:10.1016/S0926-860X(98)00264-6

Xiao, X., Sun, B., Wang, P., Fan, X., Kong, L., Xie, Z., et al. (2022). Tuning the density of Brønsted acid sites on mesoporous ZSM-5 zeolite for enhancing light olefins selectivity in the catalytic cracking of n-octane. *Microporous Mesoporous Mater.* 330, 111621. doi:10.1016/j.micromeso.2021.111621

Yarlagadda, P., Lund, C. R. F., and Ruckenstein, E. (1990). Oligomerization of ethene and propene over composite zeolite catalysts. *Appl. Catal.* 62 (1), 125–139. doi:10.1016/S0166-9834(00)82242-3

Yarulina, I., Chowdhury, A. D., Meirer, F., Weckhuysen, B. M., and Gascon, J. (2018). Recent trends and fundamental insights in the methanol-to-hydrocarbons process. *Nat. Catal.* 1 (6), 398–411. doi:10.1038/s41929-018-0078-5

Yu, L., Farinmade, A., Ajumobi, O., Su, Y., John, V. T., and Valla, J. A. (2020). MCM-41/ZSM-5 composite particles for the catalytic fast pyrolysis of biomass. *Appl. Catal. A General* 602, 117727. doi:10.1016/j.apcata.2020.117727

Zhang, Y., Wu, Q., Zhang, K., Shi, D., Jia, S., Chen, K., et al. (2023). Synergetic regulation of the microstructure and acidity of HZSM-5/MCM-41 for efficient catalytic cracking of n-decane. *Langmuir ACS J. surfaces colloids* 39 (9), 3494–3501. doi:10.1021/acs.langmuir.3c00028

Zhao, R., Haller, G. L., and Lercher, J. A. (2023). Alkene adsorption and cracking on acidic zeolites – a gradual process of understanding. *Microporous Mesoporous Mater.* 358, 112390. doi:10.1016/j.micromeso.2022.112390